NANO LETTERS

LETTER

pubs.acs.org/NanoLett

A Donor-Supply Electrode (DSE) for Colloidal Quantum Dot Photovoltaics

Ghada I. Koleilat, Xihua Wang, Andre J. Labelle, Alexander H. Ip, Graham H. Carey, Armin Fischer, Larissa Levina, Lukasz Brzozowski, and Edward H. Sargent*

Department of Electrical and Computer Engineering, University of Toronto, 10 King's College Road, Toronto, Ontario M5S 3G4, Canada

Supporting Information

ABSTRACT: The highest-performing colloidal quantum dot (CQD) photovoltaics (PV) reported to date have relied on high-temperature (>500°C) annealing of electron-accepting TiO_2. Room-temperature processing reduces energy payback time and manufacturing cost, enables flexible substrates, and permits tandem solar cells that integrate a small-bandgap back cell atop a low-thermal-budget larger-bandgap front cell. Here we report an electrode strategy that enables a depleted-heterojunction CQD PV device to be fabricated entirely at room temperature. We find that simply replacing the high-temperature-processed TiO_2 with a sputtered version of the same material leads to poor performance due to the low mobility of the sputtered oxide. We develop instead a two-layer donor-supply electrode (DSE) in which a highly doped, shallow work function layer supplies a high density of free electrons to an ultrathin TiO_2 layer via charge-transfer doping. Using the DSE we build all-room-temperature-processed small-bandgap (1 eV) colloidal quantum dot solar cells having 4% solar power conversion efficiency and high fill factor. These 1 eV bandgap cells are suitable for use as the back junction in tandem solar cells. The DSE concept, combined with control over TiO_2 stoichiometry in sputtering, provides a much-needed tunable electrode to pair with quantum-size-effect CQD films.

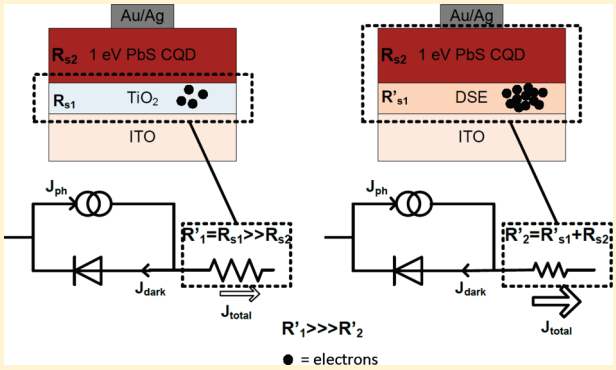

KEYWORDS: Donor-supply electrode, electron injection, charge-transfer doping, solution-processed photovoltaics, room-temperature processing

Colloidal quantum dots enable solution-processed photovoltaics capable of harvesting the full spectrum of the sun's power including the half that resides in the infrared.[1−5] Devices based on a depleted-heterojunction architecture have recently reached 6% solar power conversion efficiencies.[6−9] In the depleted-heterojunction device, a large-bandgap n-type oxide such as TiO_2 accepts photoelectrons from the p-type light-absorbing colloidal quantum dot active layer.[6,10,11] This n-p heterojunction produces a built-in field that extracts electrons from within the CQD layer, while the large valence band offset blocks holes.

Unfortunately, all reported CQD photovoltaic devices having solar power conversion efficiencies greater than 4% have relied on annealing TiO_2 electrodes at temperatures of 500 °C or greater.[6−9] High-temperature fabrication steps add to manufacturing cost and energy payback time. Steps requiring temperature treatments greater than 200 °C generally rule out the use of transparent flexible substrates desired for conformable photovoltaics.[12] Furthermore, the fabrication of multijunction photovoltaic devices based on solution-processed materials necessitates low-temperature processing of the back cell(s) for thermal compatibility with prior layers.[13]

TiO_2/PbS CQD Heterojunction Devices Based on Room-Temperature Oxide Deposition. We first attempted building electrodes at room temperature by sputtering 100 nm of TiO_2 under various Ar and O_2 concentrations onto ITO-coated glass substrates. Characterization of the materials (Supporting Information, S1) indicated that the conduction bandedge of these electrodes could be tuned through sputter conditions. A higher O_2 concentration led to a deeper electron affinity and lower doping with tuning possible from −4.0 eV down to −4.2 eV.[14]

From considerations of electron affinity depicted in Figure 1a and summarized in Table 1, we expected that these electrodes should form viable charge-separating heterojunctions when coupled to 1.3 eV-bandgap colloidal quantum dots ($\chi = -3.8$ eV[6−9]). Using the same analysis, we anticipated that only the deeper-work-function electrodes would form charge-separating junctions with 1.0 eV bandgap colloidal quantum dots ($\chi = -4.0$ eV[7,13]) of interest in small bandgap devices.[7]

These expectations were confirmed for the case of the high-temperature-processed nanocrystalline TiO_2 paired with the 1.0 eV bandgap quantum dots. With its shallow electron affinity (−3.8 eV[15,16]), the electrode forms an unfavorable band offset

Received: July 12, 2011
Revised: November 10, 2011
Published: November 15, 2011

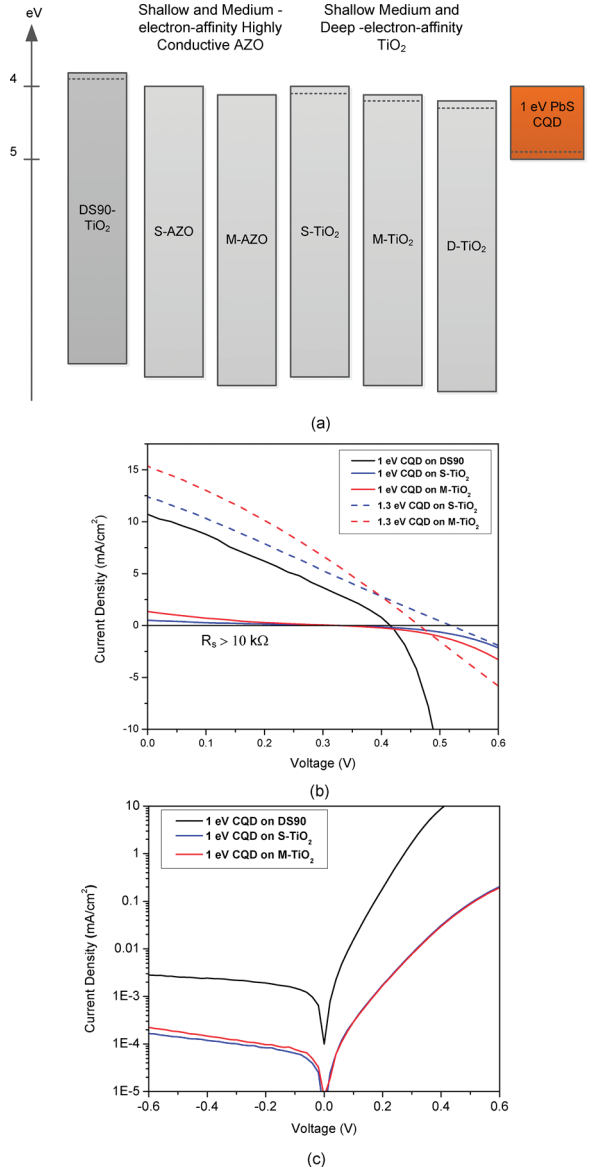

Figure 1. (a) Energy level diagram showing the highest occupied molecular orbital (HOMO) and lowest unoccupied molecular orbital (LUMO) energies of 1 eV PbS quantum dots and the band edges of the isolated TiO_2 and AZO materials with the acronyms used in this work explicitly stated. (b) $J-V$ characteristics of 1 eV CQD devices on various stand-alone TiO_2 (solid lines, DS90 vs 100 nm of S-TiO_2 and M-TiO_2) and of 1.3 eV CQD on stand-alone TiO_2 (dashed lines, 100 nm of S-TiO_2, and M-TiO_2) under AM1.5 illumination. The series resistance in the sputtered TiO_2 is in the range of 10−40 kΩ. (c) Dark $J-V$ of 1 eV CQD devices made on DS90 vs 100 nm of S-TiO_2 and M-TiO_2.

with the 1.0 eV bandgap colloidal quantum dot film. Consistent with our expectations, poor performance is observed in these devices. To further verify this picture, we investigated the dark characteristics of our devices under forward bias (Figure 1c). At high forward bias, the device shows higher majority carrier injection and 2 orders of magnitude higher current densities than the devices on the resistive sputtered electrodes. This result provides a further impetus for new electrodes suitable for photovoltaics involving small-bandgap 1.0 eV quantum dot films, the back cell in tandem colloidal quantum dot photovoltaics.[13]

In light of the above bandedge considerations, more surprising was the fact that all other devices showed poor performance compared to high-temperature-processed nanocrystalline TiO_2 controls. Especially problematic was the very large series resistance of all devices based on

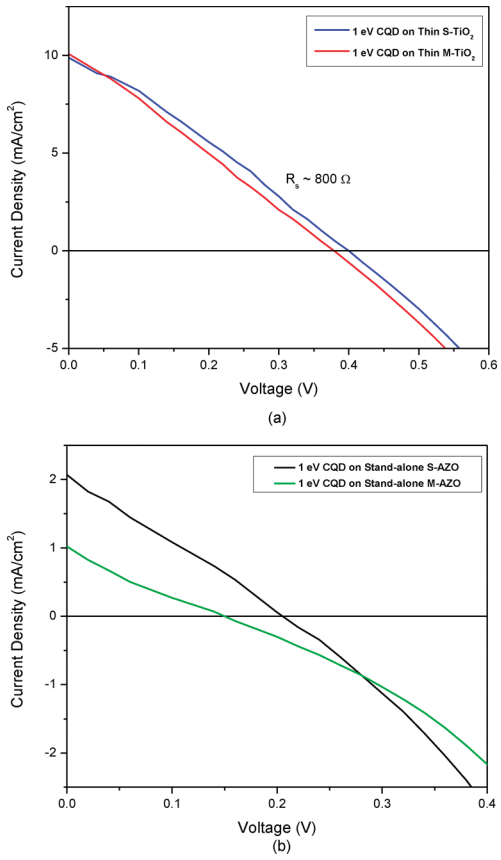

Figure 2. $J-V$ characteristics of 1 eV CQD devices on thin (30 nm) (a) S-TiO_2 and M-TiO_2. The series resistance drops to 800 ohm but is still significant. (b) S-AZO and M-AZO. Using AZO without TiO_2 leads to poor photovoltaic performance.

Table 1. Properties of electron-accepting materials[a]

Material	Acronym	Electron mobility (cm^2/V s)	Doping (cm^{-3})	Electron affinity, χ (eV)	Work function, φ (eV)	Reference
TiO_2 sputtered in Ar − shallow electron affinity	S-TiO_2	~3×10^{-5}	~7×10^{15}	4.0	4.1	Wang *et al.*[13]
TiO_2 sputtered in 1% O_2/Ar − medium electron affinity	M-TiO_2	~2×10^{-5}	~3×10^{15}	4.1	4.2	This work
TiO_2 sputtered in 3% O_2/Ar − deep electron affinity	D-TiO_2	~1.6×10^{-5}	~1.5×10^{15}	4.2	4.45	This work
AZO sputtered in Ar − shallow work function	S-AZO		>5×10^{19}[b]	>4.1[b]	4.0	Ghosh *et al.*[14]
AZO sputtered in 1% O_2/Ar − medium work function	M-AZO	10^{-2}	5×10^{19}	4.1	4.1	Wang *et al.*[13]

[a] The increase in O_2/Ar content deepens the electron affinity of the TiO_2 electrode[14,17] and the work function of the AZO. [b] AZO in pure Argon is expected to have a higher doping and higher electron affinity then AZO in oxygen content reported in ref 12; The change in electron affinity with the inclusion of oxygen during oxide sputtering is reported in refs 14 and 17.

dx.doi.org/10.1021/nl202337a |*Nano Lett.* 2011, 11, 5173–5178

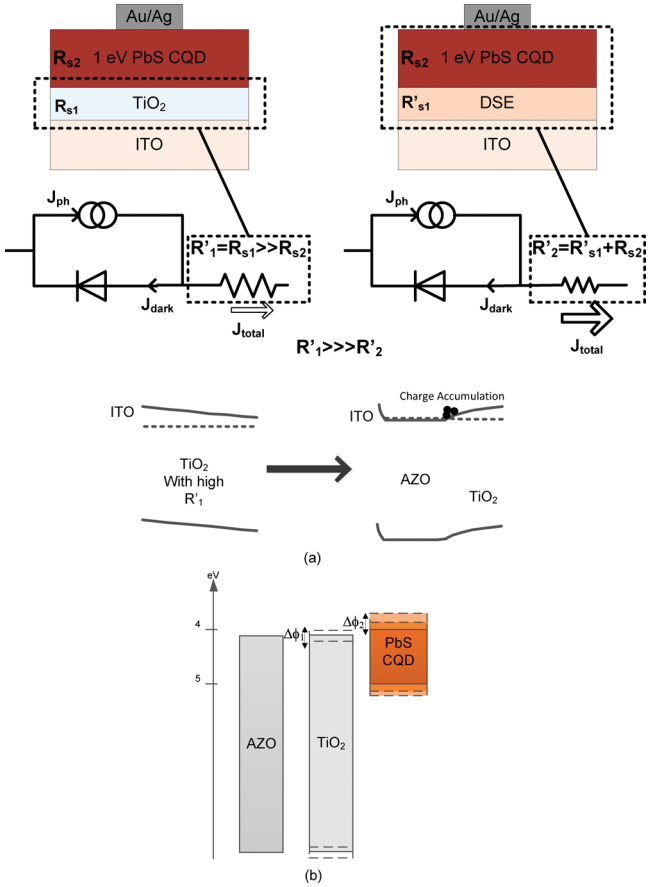

Figure 3. (a) Schematic illustrating the DSE concept: We present the 1 eV CQD device structure with an emphasis on the two-diode model of the heterojunction formed between PbS and TiO_2 before and after the application of DSE. We show that with a stand-alone TiO_2 electrode the equivalent series resistance is mainly restricted to the electrode resistance (>10 kΩ from Figure 1); the deep work function in the bottom ITO limits the performance of the device. When DSE is integrated into the device, the electrons are transferred from the now shallow work function highly doped AZO to the TiO_2. The equivalent resistance is reduced significantly. (b) Band diagram showing the relative band alignment of the AZO/TiO_2 ($\Delta\phi_1$) and the barrier height between TiO_2 and PbS CQD ($\Delta\phi_2$).

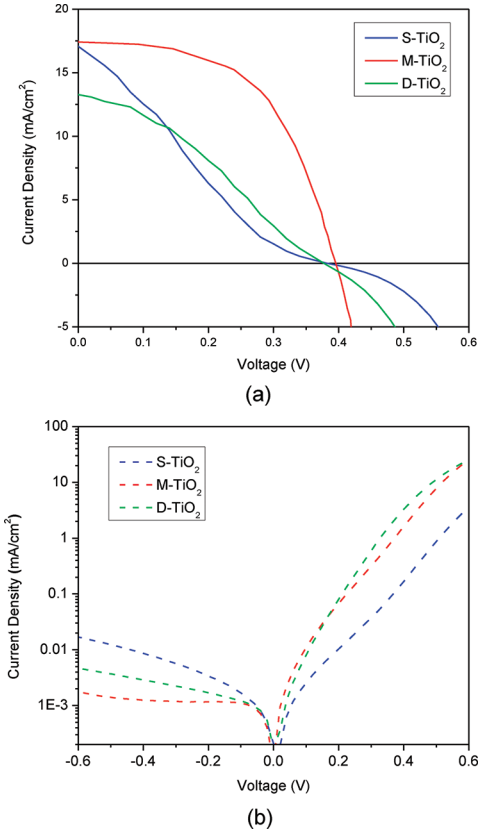

Figure 4. $J-V$ characteristics of 1 eV CQD devices on M-AZO followed by (blue) S-TiO_2 (red) M-TiO_2 and (green) D-TiO_2; M-TiO_2 is the optimal DSE with power conversion efficiency of 4%, and FF of 58% under AM1.5 illumination (a) and in the dark (b).

sputtered electrodes. This led to very poor fill factor (see Figure 1b). The electron mobility inside the sputtered oxide films[13] is known to be low (1×10^{-5} cm^2/(V s)); using a simple model (Supporting Information, S2)[18] we confirmed that a 100 nm thick layer of this material could indeed account for the observed poor performance.

We moved to much thinner coatings of the electron-accepting oxide to overcome low mobility. A 30 nm thick TiO_2 layer, the thinnest compatible with complete coverage of the underlying electrode using RF sputtering, produced an improvement over the 100 nm titania layer depicted in Figure 2a but provided a still unacceptable fill factor and overall performance.

Our models suggested that from a mobility standpoint 30 nm should have been sufficiently thin to reduce the series resistance of this layer to an insignificant level (Supporting Information, S2). However, further examination of model results revealed that when the n-type titania thickness was reduced to the point that the electron acceptor would now be fully depleted under normal photovoltaic operation, the work function in the bottom ITO electrode now began to limit the open-circuit voltage of our device (Supporting Information, S2), degrading performance unacceptably through this new mechanism.

A shallow-work-function, heavily doped electrode such as aluminum-doped zinc oxide (AZO) compatible with room-temperature sputtering should in principle resolve the preceding compromise. However, we observed negligible photovoltaic performance from all devices on the highly doped electrode AZO (Figure 2b). We interpreted the poor photovoltaic response as unfavorable interfacial junction and incompatibility of these two materials; it has been previously reported that ZnO surfaces are prone to significant chemical change in the presence of thiols. Additionally, pinning of the HOMO level of PbS CQDs has been reported at the interface with the ZnO.[19] These mechanisms are consistent with our observation of a low open-circuit voltage.

The Donor Supply Electrode (DSE) Concept. The combined failure of thick sputtered TiO_2 due to high resistance, of thin TiO_2 due to its insufficiently shallow work function, and of AZO due to materials incompatibility together led us to consider a new design for a multilayer electrode.

Combining these insights into a new electrode strategy, we took the view that immediately adjacent to the CQD layer there should be an electron acceptor having the desired electron affinity and proven chemical compatibility with the quantum dot film. Such materials are available via low-temperature sputtering as noted above (Table 1). Contacting the electron acceptor using a heavily doped, shallow work function electrode would enforce a large built-in voltage in the overall device. Desirably, if its work function was shallower than that of the electron acceptor, this conductive electrode would increase the free-carrier density in

dx.doi.org/10.1021/nl202337a |*Nano Lett.* 2011, 11, 5173–5178

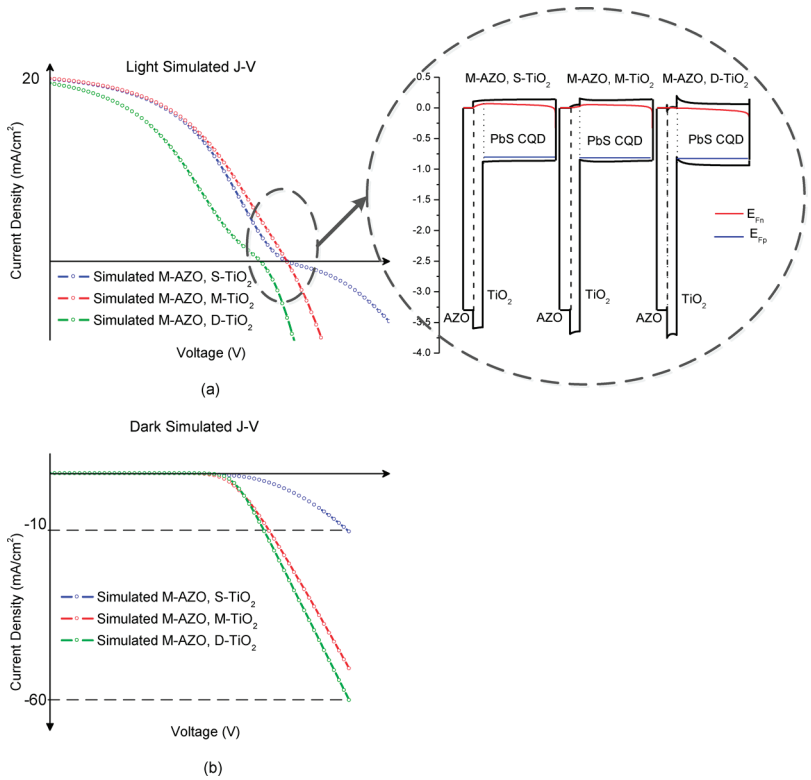

Figure 5. Band diagram near V_{oc} of 1 eV CQD devices made on M-AZO followed by S-TiO_2, M-TiO_2 and D-TiO_2 is depicted with their simulated $J-V$ characteristics in the light (a) and in the dark (b). The simulated curves are in agreement with the experimental behavior of the corresponding devices. SCAPS was used for modeling (Supporting Information, S2).

the electron acceptor via charge-transfer doping. This would offer an added benefit: it would overcome the low mobility of the room-temperature-sputtered electron acceptor by increasing its conductivity via the achievement of a high free carrier density (Supporting Information, S2).

We termed this strategy the "donor-supply electrode", or DSE and depict it in Figure 3a. We fabricated colloidal quantum dot devices atop DSEs built via all-room-temperature-sputtered AZO and TiO_2 with the latter being the topmost layer of the DSE. The light and dark $J-V$ characteristics are shown in Figure 4. The optimal DSE device achieved a short-circuit current Jsc of 17.4 mA/cm^2, an open circuit voltage Voc of 0.4 V, and a fill factor FF 58%[7,11,20] (the latter achieved via low series resistance (110 ohms) and high shunt resistance (14 kΩ)). The result was a 4% power conversion efficiency under AM1.5 100 mW/cm^2 illumination, a record for a 1 eV bandgap CQD PV device.

We now discuss in further detail the design requirements for a DSE optimally matched to the requirements of CQD photovoltaics. The charge-transfer doping concept has been employed to beneficial effect, though with a different goal, in high-electron-mobility transistors (HEMT).[21,22] HEMTs employ a heterojunction between a highly doped n-type material and a not-intentionally doped channel layer. The lack of dopant ions incorporated into the channel is conducive to high mobility, and charge-transfer from the adjacent highly n-doped layer enables control over threshold voltage.

Our DSE uses the charge-transfer doping concept for a distinct purpose. It fulfills simultaneously the requirements of

(1) room-temperature processing;
(2) carefully chosen bandedge for high J_{sc} without compromise to V_{oc};
(3) highly doped and conductive under-layer to generate an equivalent highly doped electrode.

We identify two key factors influencing the performance of our DSE-based devices (Figure 3b): the band alignment of the AZO/TiO_2 interface ($\Delta\phi_1$), and the barrier height between TiO_2 and PbS CQD ($\Delta\phi_2$).

Optimal Design of the DSE for CQD Photovoltaics. DSE charge transfer depends heavily on the band alignment of the highly doped donor layer (AZO) relative to the resistive low-doped charge-accepting layer (TiO_2). In our architecture, we expect the devices where the work function of the AZO is shallower than that of the TiO_2 to inject electrons.

We employed M-AZO ($\varphi = -4.1$ eV) as the underlayer and fabricated 1 eV PbS CQD devices with electron acceptors having three different work functions: S-TiO_2 ($\varphi = -4.1$ eV), M-TiO_2 ($\varphi = -4.2$ eV), and D-TiO_2 ($\varphi = -4.45$ eV). The best results were achieved when M-AZO ($\varphi = -4.1$ eV) was combined with M-TiO_2 ($\varphi = -4.2$ eV). Here, proximity of the TiO_2 to the AZO resulted in charge-transfer and an increase in carrier density in the TiO_2. When S-TiO_2 was employed, charge-transfer was not favored, and a poor (s-shaped) $J-V$ near open-circuit conditions was observed experimentally (Figure 4) and predicted in the model (Figure 5). This is reinforced by the low forward-biased dark current for this device, also seen both in experiment and model, explained by the resistance of the undoped TiO_2.

When D-TiO_2 is employed, band-bending becomes unfavorable in the colloidal quantum dot film from the point of view of electron extraction into the TiO_2, also resulting in a poor $J-V$ near Voc seen both in experiment and theory. Observed and modeled high forward dark current confirms that charge-transfer

dx.doi.org/10.1021/nl202337a |*Nano Lett.* 2011, 11, 5173–5178

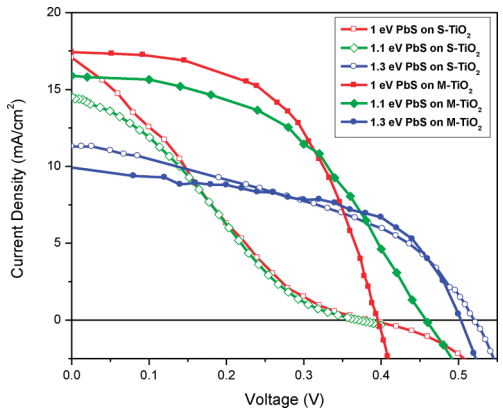

Figure 6. $J-V$ characteristics under AM1.5 illumination of 1 (red), 1.1 (green) and 1.3 eV (blue) PbS CQD devices made on M-AZO followed by both S-TiO_2 and M-TiO_2; We show that M-TiO_2 is optimal for 1.1 and 1.3 eV CQD having a deeper LUMO and thus a lower barrier height than 1.3 eV CQD.

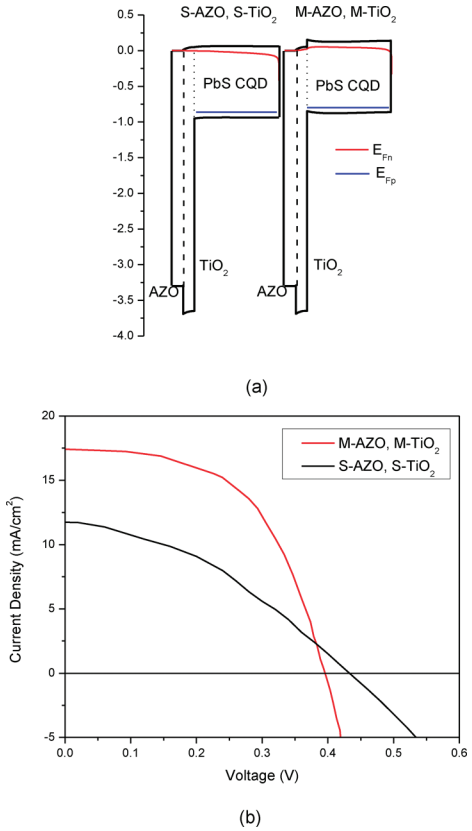

Figure 7. (a) Band diagram and (b) $J-V$ characteristics of 1 eV CQD device made on S-AZO followed by S-TiO_2 next to one made on M-AZO followed by M-TiO_2; the latter has a favorable band offset that increases carrier injection and reduces back-surface recombination.

doping was successful, and thus that the failure is instead of the barrier in the CQD film at V_{oc} conditions.

In Figure 6 we use quantum dot size-effect tuning to vary the band offset between the colloidal quantum dot film and the electron-accepting TiO_2. When larger-bandgap (1.3 eV) quantum dots are employed, the choice of electron acceptor between M-TiO_2 or S-TiO_2 has only a small influence on device response: the main effect is a slight decrease in open-circuit voltage for the M-TiO_2 relative to the S-TiO_2 case due to a sacrifice of slightly more photoelectron energy at the heterojunction. The fill factor is slightly lower due to a higher series resistance in the S-TiO_2 case. This is consistent with less efficient charge transfer from the highly doped AZO to the S-TiO_2 (Supporting Information, S2).

In the smaller-bandgap cases, a more delicate balance is found. The use of the S-TiO_2 electron acceptor not only reduces short circuit current, but also removes the charge transfer effect, leading to an unacceptably s-shaped $J-V$ characteristic. Only when the optimally aligned M-TiO_2 is employed do the 1.0 eV bandgap devices achieve their best >4% AM1.5 efficiency performance.

Figure 7 illustrates the optimal prescription for a DSE-based contact to a p-type CQD PV device. The use of a mild but still favorable band offset from the CQD layer to the TiO_2, such as 0.1 eV, aids injection of photoelectrons and minimizes bimolecular recombination (Supporting Information, S3). The use of a conductive AZO layer whose work function matches that of this TiO_2 leads to charge-transfer doping and favorable band bending including at V_{oc}. The prescription is thus:

φ (TiO_2) slightly deeper than the conduction band-edge of the CQD layer to favor injection

φ (AZO) slightly shallower than φ (TiO_2) to favor charge-transfer doping

In summary, we showed the successful utilization of the donor-supply electrode in colloidal quantum dot photovoltaics. With the insertion of a highly doped well-aligned layer beneath the resistive sputtered TiO_2, electrons from the AZO help to overcome the low doping, depletion, and low mobility seen in the thin sputtered TiO_2. The resultant electrodes are compatible with room-temperature processing, advantageous in integration with transparent flexible substrates, and with temperature-sensitive prior layers such as those employed in a tandem colloidal quantum dot solar cell. Colloidal quantum dot devices having a bandgap of 1.0 eV, suitable as the back cell in tandem photovoltaics, achieve 4% solar power conversion efficiencies and fill factor exceeding 55% when coupled to a suitably chosen DSE.

■ ASSOCIATED CONTENT

Supporting Information. Additional information and figures. This material is available free of charge via the Internet at http://pubs.acs.org.

■ AUTHOR INFORMATION

Corresponding Author

*E-mail: ted.sargent@utoronto.ca.

■ ACKNOWLEDGMENT

This publication is based in part on work supported by an award (no. KUS-11-009-21) made by King Abdullah University of Science and Technology (KAUST), by the Ontario Research Fund Research Excellence Program, by the Natural Sciences and Engineering Research Council (NSERC) of Canada, and by Angstrom Engineering and Innovative Technology. The authors would also like to acknowledge the assistance of Ratan Debnath, Huan Liu, Elenita Palmiano, Remigiusz Wolowiec, and Damir Kopilovic as well as the assistance of Mark T. Greiner with UPS/XPS measurement. G.I.K. acknowledges NSERC support in the form of Alexander Graham Bell Canada Graduate Scholarship.

REFERENCES

(1) Johnston, K. W.; Pattantyus-Abraham, A. G.; Clifford, J. P.; Myrskog, S. H.; Hoogland, S.; Shukla, H.; Klem, E. J. D.; Sargent, E. H. *Appl. Phys. Lett.* **2008**, *92*, 122111.

(2) Luther, J. M.; Law, M.; Beard, M. C.; Song, Q.; Reese, M. O.; Ellingson, R. J.; Nozik, A. J. *Nano Lett.* **2008**, *8*, 3488–3492.

(3) Tang, J.; Sargent, E. H. *Adv. Mater.* **2010**, *23*, 12–29.

(4) Tang, J.; Wang, X.; Brzozowski, L.; Barkhouse, D. A. R.; Debnath, R.; Levina, L.; Sargent, E. H. *Adv. Mater.* **2010**, *22*, 1398–1402.

(5) Choi, J. J.; Lim, Y.; Santiago-Berrios, M. B.; Oh, M.; Hyun, B.; Sun, L.; Bartnik, A. C.; Goedhart, A.; Malliaras, G. G.; Abrunal, H. D.; Wise, F. W.; Hanrath, T. *Nano Lett.* **2009**, *9*, 3749–3755.

(6) Pattantyus-Abraham, A. G.; Kramer, I. J.; Barkhouse, A. R.; Wang, X.; Konstantatos, G.; Debnath, R.; Levina, L.; Raabe, I.; Nazeeruddin, M. K.; Grätzel, M.; Sargent, E. H. *ACS Nano* **2010**, *4*, 3374–3380.

(7) Liu, H.; Tang, J.; Kramer, I. J.; Debnath, R.; Koleilat, G. I.; Wang, X.; Fisher, A.; Li, R.; Brzozowski, L.; Levina, L.; Sargent, E. H. *Adv. Mater.* **2011**, *23*, 3832–3837.

(8) Barkhouse, D. A. R.; Debnath, R.; Kramer, I. J.; Zhitomirsky, D.; Pattantyus-Abraham, A. G.; Levina, L.; Etgar, L.; Grätzel, M.; Sargent, E. H. *Adv. Mater.* **2011**, DOI: DOI: 10.1002/adma.201101065.

(9) Tang, J.; Kemp, K. W.; Hoogland, S.; Jeong, K. S.; Liu, H.; Levina, L.; Furukawa, M.; Wang, X.; Debnath, X.; Cha, D.; Chou, K. W.; Fischer, A.; Amassian, A.; Asbury, J. B.; Sargent, E. H. *Nat. Mater.* **2011**, *10*, 765–771.

(10) Debnath, R.; Tang, J.; Barkhouse, D. A.; Wang, X.; Pattantyus-Abraham, A. G.; Brzozowski, L.; Levina, L.; Sargent, E. H. *J. Am. Chem. Soc.* **2010**, *132*, 5952–5953.

(11) Gao, J.; Luther, J. M.; Semonin, O. E.; Ellingson, R. J.; Nozik, A. J.; Beard, M. C. *Nano Lett.* **2011**, *11*, 1002–1008.

(12) MacDonald, W. A.; Looney, M. K.; MacKerron, D.; Eveson, R.; Adam, R.; Hashimoto, K.; Rakos, K. *J. SID* **2007**, 15/12.

(13) Wang, X.; Koleilat, G. I.; Tang, J.; Liu, H.; Kramer, I. J.; Debnath, R.; Brzozowski, L.; Barkhouse, D. A. R.; Levina, L.; Hoogland, S.; Sargent, E. H. *Nat. Photonics* **2011**, *5*, 480–484.

(14) Ghosh, S.; Hoogland, S.; Sukhovatkin, V.; Levina, L.; Sargent, E. H. *Appl. Phys. Lett.* **2011**, *99*, 101102.

(15) Wang, X.; Koleilat, G. I.; Fischer, A.; Tang, J.; Debnath, R.; Levina, L.; Sargent, E. H. *ACS Appl. Mater. Interfaces* **2011**, *3*, 3792–3795.

(16) Tiwana, P.; Parkinson, P.; Johnston, M. B.; Snaith, H. J.; Herz, L.M. *J. Phys. Chem. C* **2010**, *114*, 1365–1371.

(17) Kim, H. S.; Jung, E. S.; Lee, W. J.; Kim, J. H.; Ryu, S. O.; Choi, S. Y. *Ceram. Int.* **2008**, *34*, 1097–1101.

(18) Burgelman, M.; Nollet, P.; Degrave, S. *Thin Solid Films* **2000**, *361−362*, 527–532.

(19) Timp, B. A.; Zhu, X. Y. *Surf. Sci.* **2010**, *604*, 1335–1341.

(20) Ma, W.; Luther, J. M.; Zheng, H.; Wu, Y.; Alivisatos, A. P. *Nano Lett.* **2009**, *9*, 1699–1703.

(21) Marso, M.; Bernát, J.; Javorka, P.; Kordoš, P. *Appl. Phys. Lett.* **2004**, *84*, 2928.

(22) Fjeldly, T. A.; Ytterdal, T.; Shur, M. Wiley & Sons: New York, 1998.